Assessment of the size window of tumor vascular permeability using dextran-based CEST MRI

Yuguo Li^{1,2}, Kannie Chan^{1,2}, Yuan Qiao³, Jiadi Xu², Jeff Bulte¹, Bert Vogelstein³, Michael McMahon^{1,2}, Shibin Zhou³, Peter van Zijl^{1,2}, and Guanshu Liu^{1,2}

¹Radiology, Johns Hopkins University School of Medicine, Baltimore, MD, United States, ²FM Kirby center, Kennedy Krieger Institute, Baltimore, MD, United States, ³Ludwig Center, Howard Hughes Medical Institute and Sidney Kimmel Cancer Center, Johns Hopkins University School of Medicine, Baltimore, MD, United States

Target audience: Physicians and investigators who are interested in assessing the vascular permeability of tumors.

Purpose: To exploit natural dextrans (**Fig. 1a**) as MRI contrast agents for assessing the size window of tumor vascular permeability, which has applications for clinical diagnostics and for developing nanoparticulates of appropriate sizes to maximize their tumor targeted delivery for treatment¹.

Methods: Dextrans of molecular weight (MW) = 9.5, 70, 200 and 2000 kD and D-glucose were prepared at a concentration of 5 mg/ml (28 mM per glucose unit) in PBS buffer (pH=7.3) and assessed for their CEST contrast on a vertical bore Bruker 11.7 T MRI scanner equipped with a 15 mm volume coil as described previously.³ *In vivo* MR studies were carried out on a Biospec11.7 T horizontal MRI scanner equipped with a 23 mm mouse brain volume coil. MR images were acquired according to the protocol in Fig. 2a to monitor the changes in CEST contrast upon i.v. injection of dextran to Balb/c mice bearing CT26 colon tumors in the flank (~350 mm³, 14 days after the implantation of $5x10^6$ CT26 cells). Details of the MRI study are provided in the caption of **Fig. 2**. Data were processed using custom-written MATLAB scripts. After correcting for B_0 inhomogeneity using the WASSR method, the *in vivo* CEST contrast was quantified by averaging the MTR_{asym}=(S^{III})/S₀ from 0.8 to 1.2 ppm.²

Results: In vitro phantom studies (Fig. 1b) revealed that different MW dextrans and glucose share a similar CEST contrast pattern, e.g. resonant at ~1 ppm when B_1 =3.6 μT was used. Similar to glucose, dextrans also exhibit a highly B₁-dependent CEST pattern (Fig. 1c), with signal increasing at higher B₁ for the fast exchanging OH protons. The apparent shift of the curve to higher frequency is due to broadening of the direct saturation and not a real effect. Fig. 1d shows that ~5% CEST contrast can be generated per 3 mM glucose unit concentration, which, for example, corresponds to ~0.3 µM dextran for a MW of 200 kD. As a first in vivo demonstration, we injected two dextrans (9.5 and 70 kD, 4 and 14 nm in radius respectively) to mice bearing CT26 tumors to assess the differential permeability of the tumor to particles of different sizes. Because low MW dextran will be quickly cleared from plasma and tumor according to the literature⁴, we injected the low MW dextran first (Fig. 2a), followed by the high MW dextran after a sufficiently long interval (e.g. > 40 min). This allowed detection of the pharmacokinetics of both dextrans in the same tumor within a single MRI session. Fig. 2b shows the CEST contrast maps at different time points before and after injection. To better show the CEST enhancement, we also display Δ MTR_{asym} at different time points in specific tumor and kidney regions (Figs. 2c & 2d). The results clearly show a differential vascular permeability of the studied tumor to dextrans of different sizes, with 10 kD dextran (~4 nm) penetrating deeply into the tumor while 70 kD dextran (~14 nm) only accumulates in the tumor periphery. Interestingly, the contrast enhancement obtained by 70 kD dextran was similar to the Gd-enhanced image (Fig. 2b). As expected, dextran of 4 nm size was cleared through kidney, as evidenced by the continuously increasing CEST contrast in kidney after injection (Figs. 2c & 2d).

Discussion: The particle size (diameter) of dextran has been well studied, i.e. 4, 14, 20 and 54 nm for MW = 9.5, 70, 200 and 2000 kD respectively 5 , which enables the exploitation of dextrans of different MW to assess the window of tumor vascular permeability. Here, we showed that CEST MRI could be used to assess the differential permeability of the tumor to 9.5 kD dextran (4 nm), and 70 kD dextran (14 nm). It should be noted that the size of 70 kD dextran is slightly above the critical size to have an Enhanced Permeability and Retention (EPR) effect (i.e. > 12 nm in diameter) Investigation on dextrans

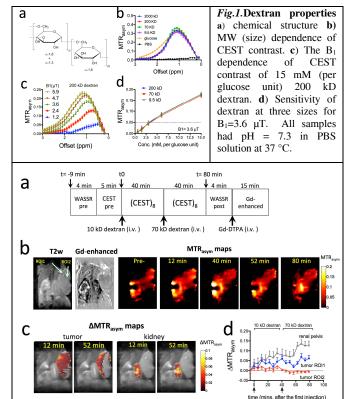


Fig. 2. In vivo CEST MRI of dextran uptake in tumor and kidney. a) Imaging protocol. b) T2-w, Gd-DTPA enhanced T1-w, and CEST contrast maps at different time points. c) The Δ MTR_{asym} maps of only tumor and kidney at 17 minutes and 57 minutes after the experiment started (12 minutes after the injection of 10 kD or 70 kD dextran). d) Change of mean ROI CEST contrast in the two tumor ROIs and the renal pelvis. The changes were quantified by $\Delta MTR_{asym}(t) = MTR_{asym}(t)$ -MTR_{asym} (t0). Methods: a pre-scan was acquired using a segmented CEST acquisition with offsets ranging from 0.4 to 1.6 ppm (step=0.2 ppm). Mice were injected i.v. with 300 μL 10kD dextran PBS solution (size~4 nm, 375 mg/kg bw) followed by eight repeated segmented CEST acquisitions. Then 300 µL 70kD dextran solution was injected at the same dose and imaging repeated. Each acquisition took ~5 minutes. A fatsuppressed RARE sequence with a continuous wave pre-saturation pulse B1=1.8 μT and 3 seconds (TR/TE=5000/5 ms, RARE factor=10)² was used. After CEST acquisition, contrast enhanced images were acquired using a T1-w spin echo sequence (TR/TE=500/10 ms) before and 15 minutes after i.v. injection of Gd-DTPA (0.5 mmol/kg; 0.1 ml bolus over about 3 s).

of larger sizes is ongoing. Because dextrans are FDA approved and already used clinically, this approach has high translatability potential.

Conclusion: We characterized the CEST properties of dextrans of different MW, and demonstrated their usefulness in delineating the size window of tumor vascular permeability.

References: (1) Chauhan, V. P.; Stylianopoulos, T.; Martin, J. D., et al. Nat Nanotechnol **2012**, 7, 383-8.(2) Chan, K. W.; McMahon, M. T.; Kato, Y., et al. Magn. Reson. Med. **2012**, 68, 1764-73. (3) Liu, G.; Gilad, A. A.; Bulte, J. W., et al. Contrast Media Mol. Imaging **2010**, 5, 162-70.(4) Dreher, M. R.; Liu, W.; Michelich, C. R., et al. J. Natl. Cancer Inst. **2006**, 98, 335-44. (5) Armstrong, J. K.; Wenby, R. B.; Meiselman, H. J.; Fisher, T. C. Biophys. J. **2004**, 87, 4259-70. This work is supported by NIH grants R21EB015609, R01EB015032 and R01EB012590.